Chapter 6

Rotation of ^{92}Nb nucleus about intermediate principal axes

6.1 Introduction

Having observed collective $M1$ bands in ^{93}Nb we decided to probe high-spin states in ^{92}Nb. While doing so, we observed discrepancies in earlier literature by Zheng *et al*, [10]. So we investigated the nucleus ^{92}Nb. Nuclei in the neighborhood of semi-magic shell closures $Z \approx 40$ and $Z \approx 50$ constitute a laboratory to study single-particle excitations as well as high-spin states based on collective phenomena. This may provide a suitable testing ground to understand interactions involved as well as various shape parameters as a function of angular momentum and excitation energy [11, 145, 161, 176–179]. Several efforts have been made to describe the low-lying states in this mass region within the shell model framework [169, 180–182] which were later extended to explain the medium and high-spin region, using different model spaces and interactions in ^{88}Y, ^{89}Zr, ^{90}Nb, ^{91}Mo, ^{92}Tc and ^{92}Nb [10, 81, 145, 148, 177, 178, 181, 183, 184] to unveil the overall nuclear properties.

This mass region also provides an opportunity to study the high-spin states beyond the shell closures through the core breaking mechanism [169, 185–190]. The excited states of these nuclei have attracted a lot of attention in theoretical and experimental works. The existence of one odd neutron outside $N = 50$ motivated various research groups

to investigate the nuclei in the isotonic $N = 51$ chain up to relatively high-spin states [5, 6, 81, 135, 190–194]. As the last valence proton and neutron may occupy different Nilsson orbits near the Fermi surface, the evolution of a variety of structures may help in understanding the coupling modes of two non-identical nucleons [195]. The occupation of shape-driving orbitals at higher spin gives rise to the emergence of a regular band structure with increasing excitation energy. With one neutron in the $d_{5/2}$ orbital, high-spin states in the $N = 51$ nuclei can be understood by the interplay between the ($f_{5/2}$, $p_{3/2}$, $p_{1/2}$) $\rightarrow g_{9/2}$ proton excitations, $g_{9/2} \rightarrow (d_{5/2}, g_{7/2})$ neutron-core excitations or $(d_{5/2} \rightarrow g_{7/2})$ neutron excitations, and recouplings of the $g_{9/2}$ valence protons. Such states in near-spherical nuclei can help understand the emergence of collectivity as a function of angular momentum and the alignment characteristics of valence shell nucleons. Observations of $M1$ transitions were reported by Funke *et al.* [196] instead of $E2$ bands in ^{89}Y, which is dominated by one-proton hole below semi-magic number 40. Further, angular momenta in the states beyond excitation energy of 4 MeV were reported to be generated more favorably with the alignment of neutrons obtained by breaking the magic shell closure of 50. Lifetime measurements using the fast $M1$ transitions further strengthen the evidence for neutron core excitations [196]. Similarly, ^{89}Zr is another example of a one-proton hole system where a high-spin dipole band with enhanced $M1$ transitions and very weak $E2$ cross-overs were reported. Interestingly, cranked-Nilsson Strutinsky calculations (CNS) revealed that rotation of the weakly deformed triaxial ^{89}Zr nucleus about the classically unfavored longest possible principal axis can generate such dipole bands. It is already established that nuclei with dominance of holes would consist of structures based on the longest axis rotation of the nucleus [7]. Further, regular dipole band structures have been observed at high spins in nuclei with neutron shell-closure such as ^{88}Sr [197], ^{86}Kr [198] and ^{90}Zr [8, 199] nuclei. These band structures have been successfully described involving

excitations of protons to the $g_{9/2}$ orbital and neutrons to the $d_{5/2}$ orbital across the $N = 50$ shell closure.

The low-lying as well as medium to high-spin states in ^{92}Nb have already been reported by many groups over the past many years [10, 81, 139, 148]. The observation of collective bands in such nuclei should be indicative of the corresponding nuclear shape with specific deformation parameters. A few collective structures in ^{92}Nb were reported in earlier literature. However, the spin and parity of the corresponding states in those bands were tentatively assigned. According to Zheng *et al.*, the negative parity ($M1$) band 1 with comparatively high intensity is fed to the low-spin levels of ^{92}Nb mostly through high-energy weak transitions. At the same time, a decay channel was proposed from the level at 5504.0- (from band 1) to 3325.0-keV (at $I = 13^{+}$). However, no such transition was experimentally observed or traced because of a lack of observed coincidence between 628.8- and 1304.9-keV transitions with the 1550.5-keV transition.

Therefore, it should be interesting to review the level structure of ^{92}Nb so that band 1 could be placed with a confirmed band head and feeding transitions to the low-spin regime. Further, the present work confirms the spin and parity of the states in band 1. In addition, the present work reports a new $M1$ band situated almost at a similar excitation energy and angular momentum as band 1. Efforts have also been made to review the nucleon-nucleon interaction in such nuclei through shell model calculations. Finally, CNS model calculations have been implemented to conclude about the possible nuclear rotations at high spin.

6.2 Experimental details and analysis

High-spin states in the ^{92}Nb have been populated using the reaction ^{80}Se(^{18}O, $p5n$)^{92}Nb at a beam energy of 99 MeV. The ^{18}O beam from 14UD pelletron-linac accelerator was bombarded on 1.4 mg/cm^2 ^{80}Se with a backing of 1.5 mg/cm^2 ^{27}Al. The γ-rays were

detected with the Indian National Gamma Array (INGA) at TIFR [61]. Further details can be found in Ref. [111].

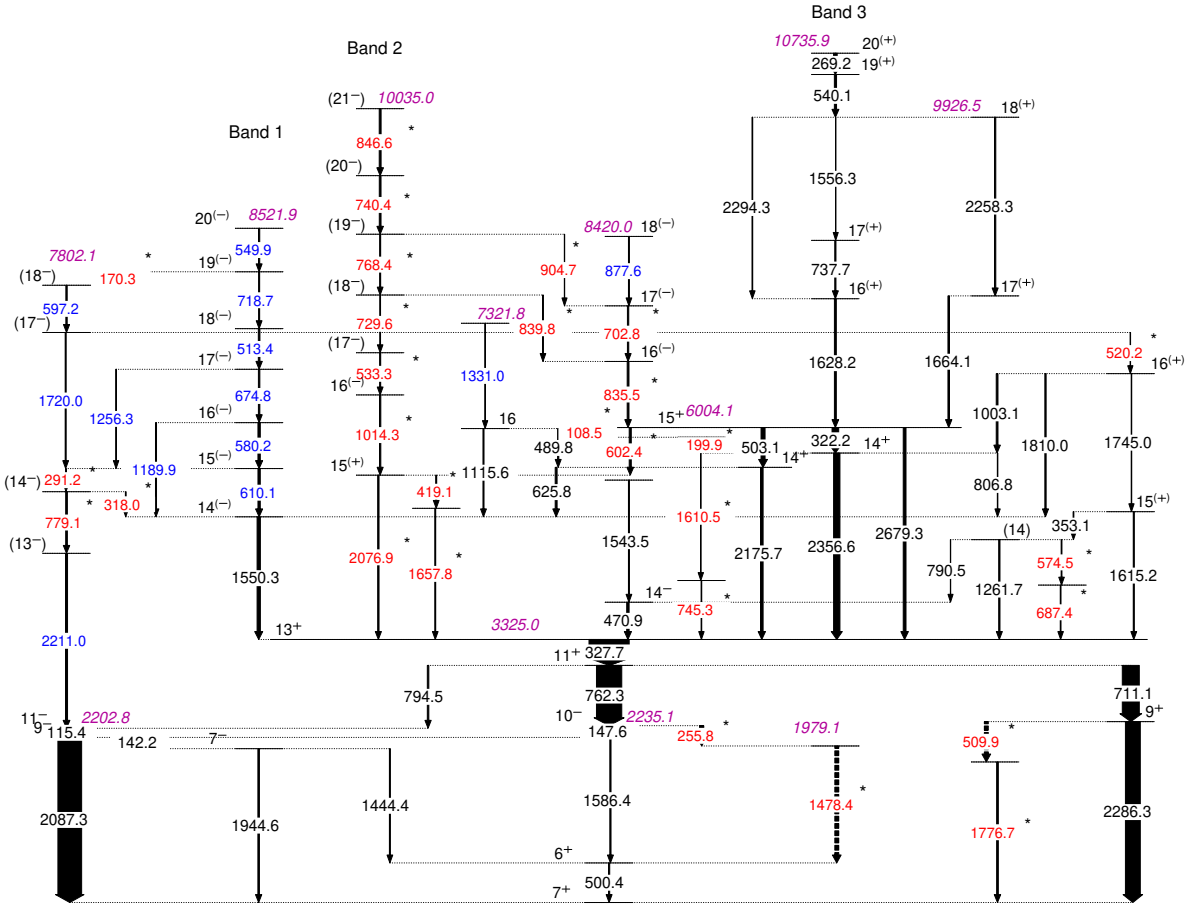

Figure 6.1 The level scheme of ^{92}Nb. Newly observed gamma transitions are marked by red labels, while rearranged transitions are indicated in blue. The thickness of the arrow represents the relative intensity of the gamma rays as mentioned in A.5.

6.3 Results and Level Scheme

The level scheme of ^{92}Nb incorporating γ transition properties like energies, intensities, and spin-parity as enlisted in Table A.4 is shown in Fig. 6.1. The entire level scheme is established using the information of γ-γ coincidence and intensities of the respective γ transitions. The width of the arrows across each transition measures its relative intensity

with respect to 327.7-keV γ ray, whose intensity has been normalized to 100. Spin assignments have been done based on multipolarity which is measured through angular distribution ratios. In some cases, the presence of interconnecting transitions or parallel feeding patterns to other levels helps us to confirm the spin. The parity assignments to the levels in the lower part of the level scheme have been adopted from the previous works [10, 81, 139].

The low-spin part of the level scheme was established by Brown *et al.* [81]. The level scheme was further developed by Yi-Heng *et al.* [139], Zheng *et al.* [10] and Ren *et al.* [148]. Most of the γ rays reported in the previous works were confirmed. Although the transitions with energies of 90, 123, 150, 164, 194, and 254 keV, which lie between the low-energy levels established by Brown *et al.* [81] were not observed in this study. Owing to the fusion-evaporation reaction using a lighter beam and probable transfer reaction, the low-lying states are expected to be more populated in the work by Brown *et al.* [81]. A similar light-ion reaction was recently used by Ren *et al.* [148] to discuss many newly observed transitions decaying from lower excited states in the framework of shell model calculations. The transitions with energies of 628.8-, 1095.3-, 1304- and 1190.7-keV were reported by Zheng *et al*. [10] was not convincingly observed in the present work. In the recent study by Ren *et al.* [148], which employed the same reactions as in Ref. [10] and Ref. [139], the high-spin states of ^{92}Nb were revisited. It is worth noting that the high-spin level structure in ^{92}Nb has not been extended much by Ren *et al.* [148] compared to the earlier works by Zheng *et al*. [10]. In this work, a very few weak transitions, such as 862 and 881 keV, were not observed. However, these were reported to decay from band 3 to band 1 (see [148]). A spectrum with a gate on 2087.3-keV transition shows the γ rays belonging to the lower part of the level scheme (see Fig. 6.2). Further, some of the newly placed transitions depopulating the high-spin level as well as the transitions belonging to band 1 and band 2, can also be seen in the figure.

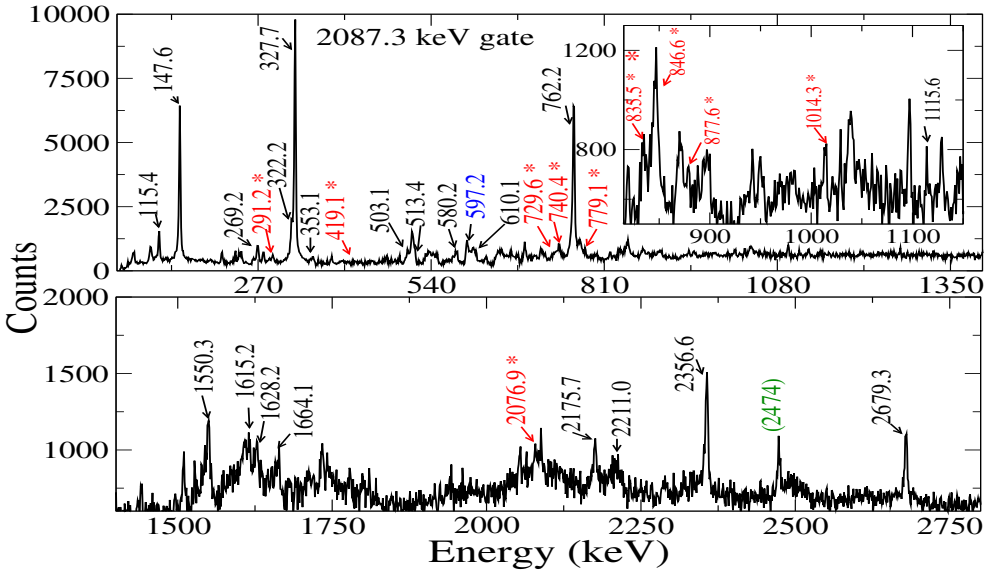

Figure 6.2 γ-γ coincidence spectrum gated on 2087.3-keV transition. Transitions marked with * are newly observed ones. Transitions constituting band 1 and band 2 have been shown in the spectrum. The peak with parentheses is contamination.

The tentatively assigned spin and parity for most of the previously reported transitions by Zheng *et al.* [10] was confirmed in this work. The transitions 2356.6 and 2175.7 keV were reported as stretched quadrupole $E2$ transition in the previous work [10], but the value of the angular distribution ratio (R_θ), which is 0.7(1) for the 2175.7-keV transition and 0.8(1) for the 2356.5keV transition led us to conclude that 2356.6- and 2175.7- keV transitions exhibit dominant characteristic of a stretched dipole $M1$.

Assignment of multipolarity to both the transitions of 2356.6 and 2175.7 keV is also in agreement with the stretched quadrupole $E2$ nature of 2679.3-keV transition and stretched dipole $M1$ character of 322.2- keV γ ray. It is to be highlighted that the transition with 2679.3 keV energy has been shown as a connecting transition between the 13^+ and a suggested 16^+ according to the Ren et al. [148]. This would then assign $M3$ multipolarity to the 2679.3-keV transition and hence this possibility can essentially be excluded.

The level scheme has been further extended with the help of twenty-nine new transitions. New transitions have been placed in low- as well as high-spin regions. A negative parity

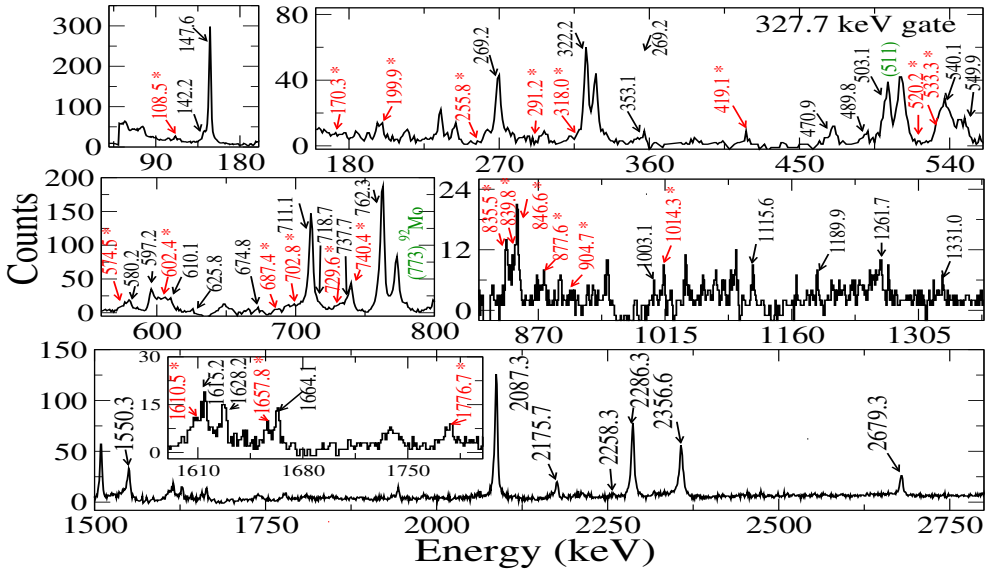

Figure 6.3 γ-γ coincidence spectrum gated on 327.7-keV transition. Transitions marked with * are newly observed ones. Peaks with parentheses are contamination.

band (band 2) was established for the first time. The spectrum gated on 327.7- keV clearly shows most of the newly observed transitions placed in the level scheme (see Fig. 6.3).

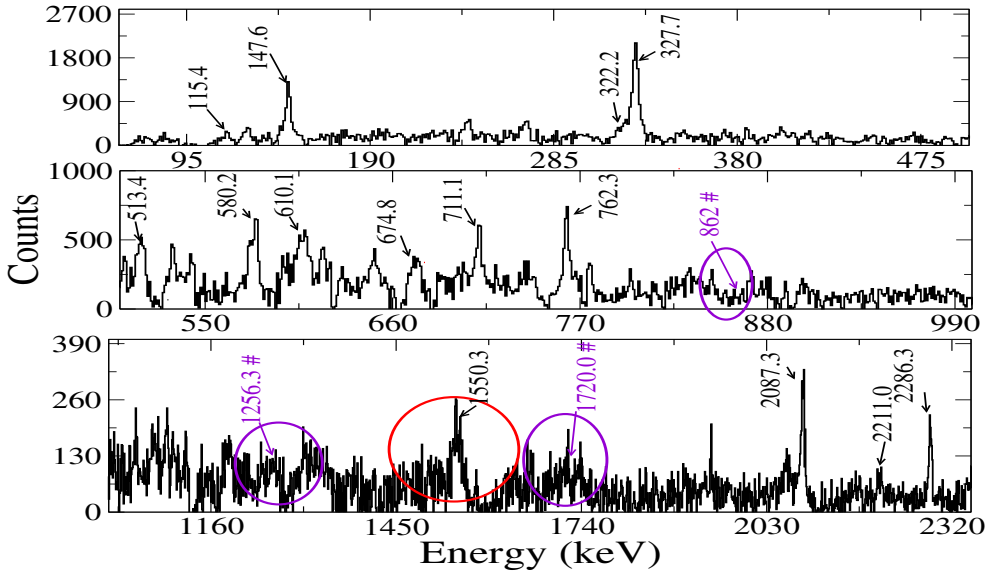

Figure 6.4 γ-γ coincidence spectrum gated on list of 549.9-,718.7-, 674.8-, and 513.4-keV transitions.

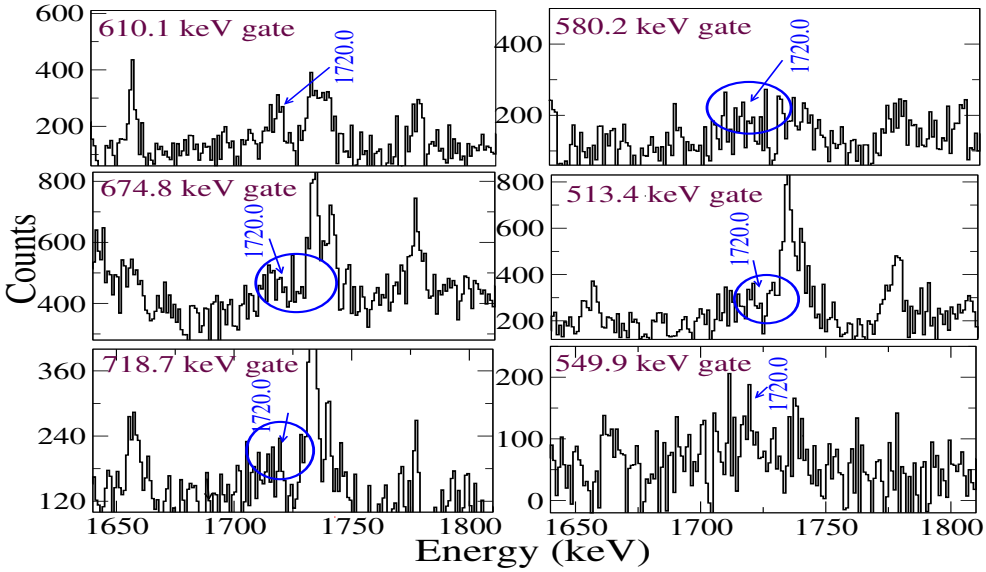

Figure 6.5 γ-γ coincidence spectrum gated on 610.1-, 580.2 574.8-,513.4.7-, 718.7-, and 549.9-keV transition.

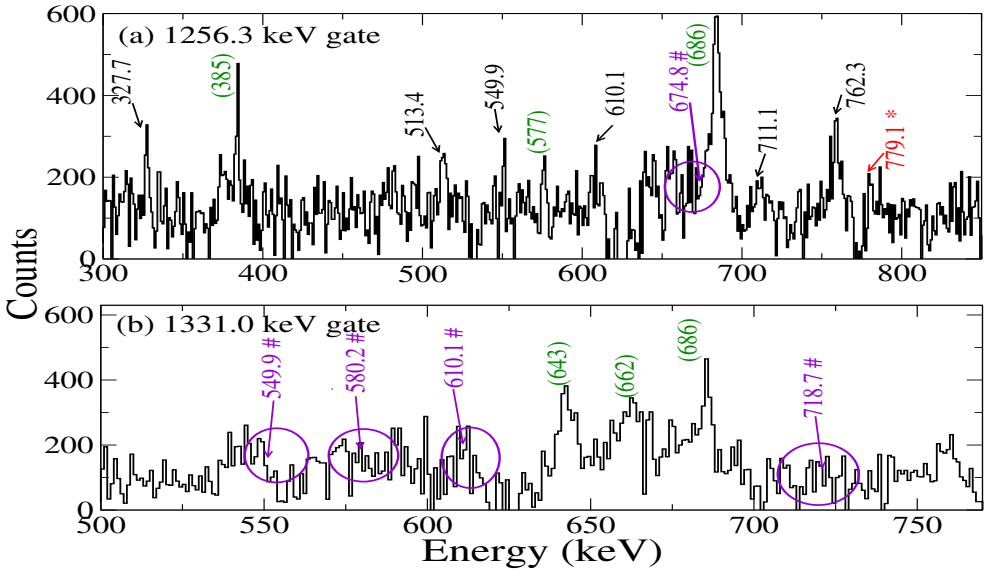

Figure 6.6 γ-γ coincidence spectra gated on (a) 1256.3- and (b) 1331.0-keV transitions. Transitions marked with * are newly observed ones. Transition marked with # has been placed by Zheng *et al.* [10] which were not observed in the present work. The present study provides clear evidence for the absence of a 674.8 keV in the 1256.3 keV gate and 549.9-,580.2-,610.1-, and 718.7 keV in the gate 1331.0 keV transition. Peaks with parentheses are contamination.

In the present work, we confirmed the presence of a 1550.3-keV transition above the γ ray with an energy of 327.7 keV. Currently, the calculated polarization asymmetry parameter, Δ_{assym}, is positive at 4.7(43) $\times 10^{-2}$, indicating the electric nature of the 1550.3-keV transition. Consequently, state 14 is classified to have negative parity based on the Δ_{assym} value. However, the uncertainty in the measured value is large and therefore, there is a small probability for the Δ_{assym} to swing to the magnetic type. Hence, the parity of the states in band 1 is reported tentatively. The band 1 was placed on the $14^{(-)}$ state (see Fig. 6.1) since the transitions 1256.3, 1331.0 and 1720.0 keV have not been observed in coincidence with band 1 in the present work (see the discussion below with Fig. 6.5,6.6).

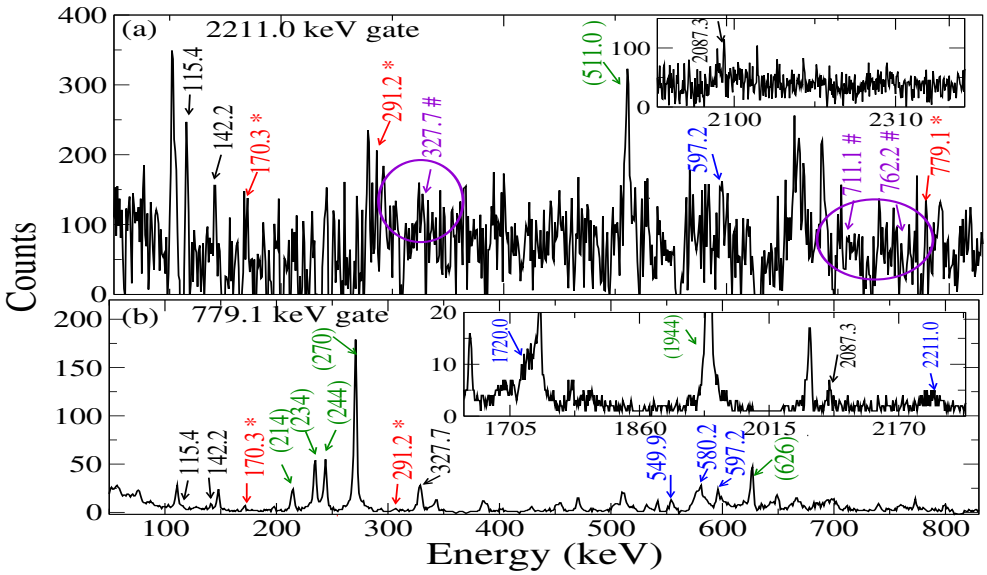

Figure 6.7 γ-γ coincidence spectrum gated on (a)2211.0- and (b)779.1-keV transition. Transitions marked with * are newly observed ones. Peaks with parentheses are contamination.

Spectrum gated on the list of 549.9-, 718.7-, 513.4-, and 674.8-keV transitions from band 1 is shown in Fig. 6.4. This spectrum clearly shows all the transitions, viz. 513.4, 580.2, 610.1 and 1550.3 keV of band 1 and corresponding connecting transitions to the lower half. It is to be mentioned that the transitions 862.0, 1256.3 and 1720.0 keV marked with # are not observed in this spectrum, see Fig. 6.4. The spectrum gated on the transitions

at 1256.3 keV and 1331.0 keV indicates that these transitions do not coincide with band 1, as illustrated in Fig. 6.6, which is contrary to the observations made in [10]. Therefore, the band has been placed upon the 1550.5 keV level with certainty. On the other hand, 1331.0-keV γ ray has been observed in coincidence with 1115.6 keV which feeds on top of 1550.3-keV transition. In turn the depopulating level of 1115.6-keV γ is further decayed through a parallel cascae consisting of 489.8- and 625.8-keV transitions.

The transition with energy 2211.0 keV is displaced on top of the 2202.8-keV state [111]. One weak cascade of a couple of transitions 779.1 and 291.2 keV has been placed above the 2211.0-keV transition. These two transitions connect band 1 with the 2211.0-keV transition, whereas 1720.0-keV is placed on top of 291.2-keV γ ray (Fig. 6.7). Previously reported 597.2-keV transition [10] is now placed above the 1720.0 keV transition at (17^{-}) state which is connected to the $19^{(-)}$ state of band 1 through 170.3-keV transition, see Fig. 6.1.

A weak 2076.9-keV transition has been placed at medium spin above 13^{+} state, parallel to the 1550.3-, 2175.7-, and 2356.6-keV $M1$ transitions. Based on the value of R_θ of this transition, we have assigned the spin $15^{(+)}$ to this level. A couple of transitions with energy 1657.8- and 419.1-keV have been placed parallel to the 2076.9-keV transition.

A transition 1014.3 has been placed at 5402.1-keV level above the 2076.9-keV transition. The value of R_θ and Δ_{assym} show (see Table A.4) the $E1$ nature of 1014.3-keV transition. The gated spectrum with gate 2087.3 keV and sum gate on 711.1- and 2286.6-keV transitions shows the 2076.9-keV γ ray belongs to band 2 (see Fig. 6.2 and Fig. 6.8(a)).

The newly placed band 2 with band head at (16^{-}) is placed on top of 13^{+} state through 2076.9- and 1014.3-keV transitions. The band was established up to the $I^{\pi} = (21^{-})$ level at 10035.0 MeV. This band contains five transitions 533.3, 729.6, 768.4, 740.4, and 846.6 keV. A spectrum gated on 2076.9-keV transition is shown in Fig. 6.8(b). The members of

this band are visible, besides several previously known low-lying transitions with energies of 147.6, 711.1, 762.3, 2087.3, and 2286.3 keV are also clearly observed (see Fig. 6.8(b)). The spin and parity of the levels of the band are tentatively assigned due to the weak

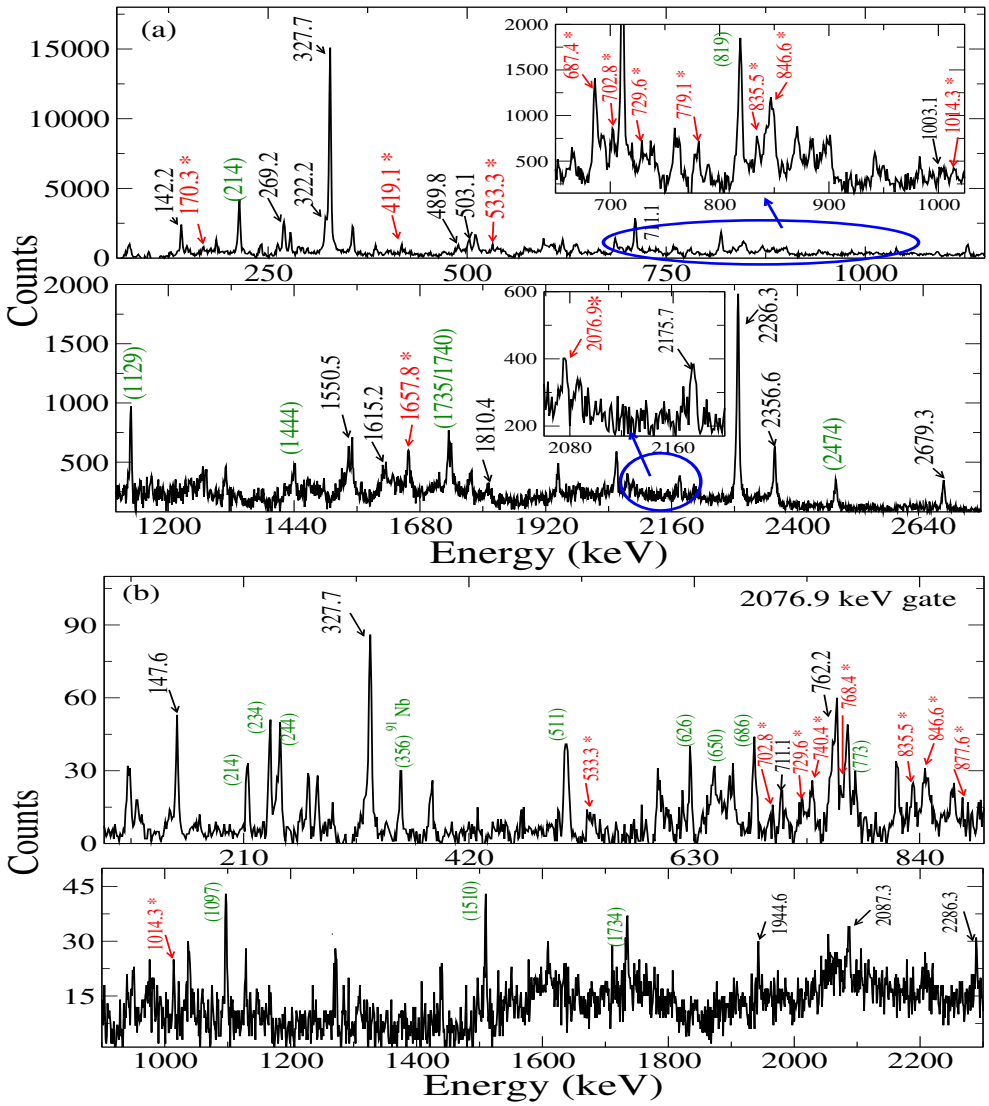

Figure 6.8 γ-γ coincidence spectrum (a)with sum gate on 711.1- and 2286.6-keV spectrum gated on (b) 2076.9-keV transition. Transitions marked with * are newly observed ones. The lower panel shows a couple of ground-state transitions. Peaks with parentheses are contamination

intensity of the transitions and the contaminant γ rays. The R_θ ratio measured for the 1014.3 keV γ ray connecting to band 2 shows its dipole nature. Another sequence, which is

designated as band 3, has already been observed by Zheng *et al.* [10]. The transitions with energy 503.1, 1628.2, 737.7, 1556.3, 540.1 and 269.2 keV constitute this band (see Fig. 6.3). A parallel sequence consisting of 2258.3- and 1664.1-keV transitions decays from 9926.5-keV level to 6004.1-keV state at 15^+. The spin of the levels of this band was also confirmed. A stretched $E1$ transition with energy 470.9-keV depopulates the 3795.7-keV level which was previously reported by B.A. Brown [81] though not reported by Zheng *et al.*. The transition 1543.5 keV decays onto a 3795.7 keV state. The sequence of transitions 745.3, 1610.5, 199.9 and 108.5-keV has been placed at 3325.0-keV state parallel to the 1550.3 and 1115.6-keV γ- ray. An interconnecting 602.4-keV transition has been placed at spin between 15^+ and $15^{(+)}$ state parallel to the 503.1-keV transitions. A sequence of transitions 835.5, 702.8 and 877.6 keV has been placed on the top of the 6004.6 keV level. Interconnecting transitions 904.7- and 839.8-keV connect band 2 to the 835.5-keV transition.

A couple of transitions at 574.5 and 687.4 keV are placed parallel to the 1261.7-keV transition above the 13^+ state. The depopulating level of 1261.7 keV further branches out through 790.5 keV that feeds 470.9-keV transition. The state 13^+ is also fed by a weaker cascade of three transitions viz. 520.2, 1745.0, and 1615.2 keV which also connects $I = 15^{(+)}$ to $I = (14)$ through 353.1-keV transition. The partial intensity of 520.2-keV transition also feeds on top of 2356.6-keV transition through 1003.1-keV γ ray and 1550.3-keV transition through 1810.0-keV γ ray.

A few new transitions are also placed in the low-spin regime of the level scheme. The 2286.3-keV ground state transition is associated with an alternative decay path hosting 509.9- and 1776.7-keV transitions. Similarly, 255.8 and 1478.4 keV are placed according to the observed coincidences.

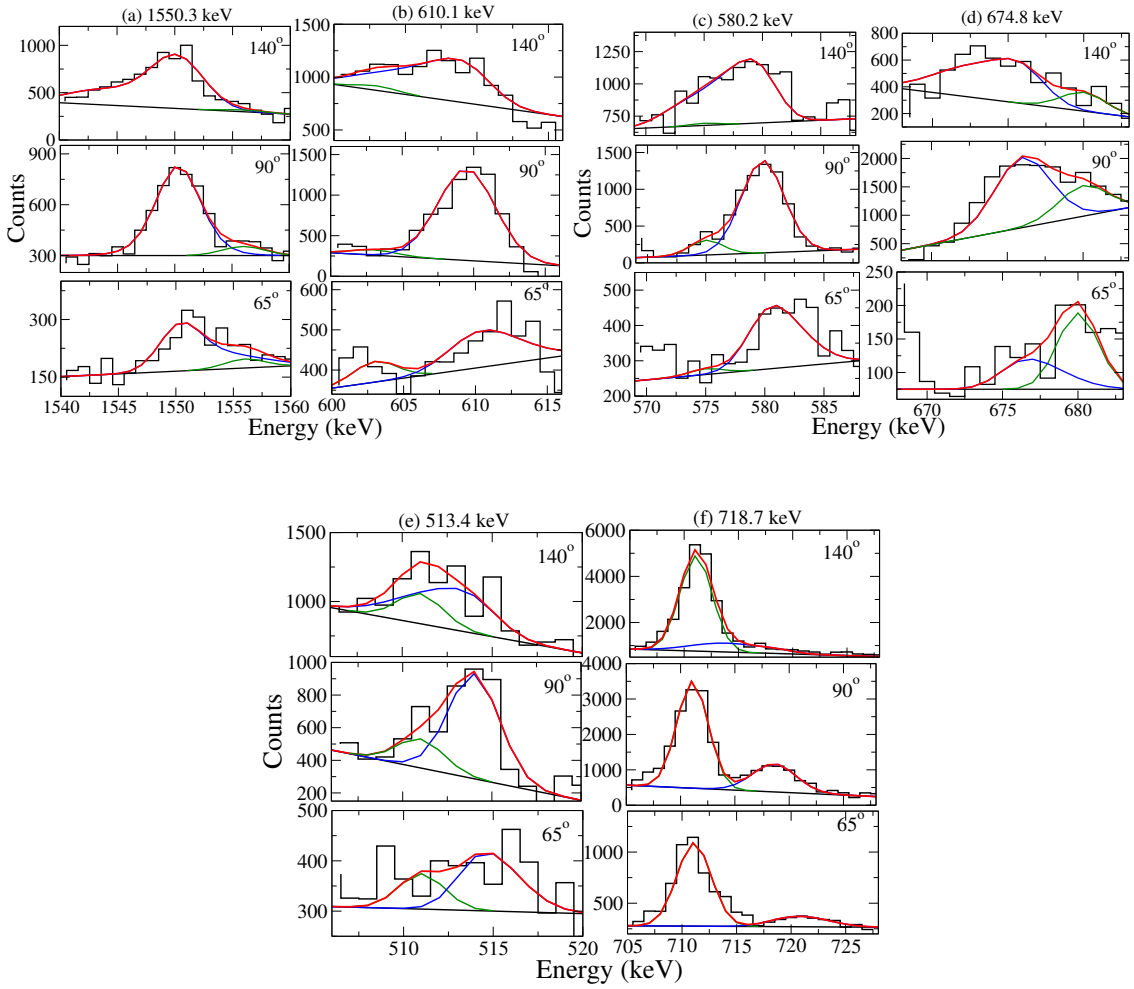

Figure 6.9 Representative spectra along with theoretically fitted lineshapes for (a) 1550.3 keV, (b) 610.1 keV, (c) 580.2 keV, (d) 674.8 keV, (e) 513.4 keV and (f) 718.7 keV dipole transitions in the dipole band of ^{92}Nb. The upper, middle and lower rows correspond to the shapes in the 140°, 90° and 65° detectors, respectively. The blue, green, and red curves represent the desired lineshapes of gamma transitions, contaminant peaks, and total lineshapes.

6.3.1 Lifetime measurements through DSAM

The measurement of level lifetimes has been separately categorized for the negative-parity dipole band 1 feeding on top of the 13^+ state. The Doppler-shifted spectra were generated from the asymmetric matrices with a gate on 327.7-keV γ ray. Representative lineshape spectra of 1550.3-, 610.1-, 580.2-, 674.8-, 513.4- and 718.7-keV transitions observed at 140°, 90°, and 65° angles are displayed in Fig. 6.9. We were able to extract lifetimes for only six states in the band. The results are summarized in Table 6.1. The top transition, i.e., 718.7 keV, was fitted assuming 100% side feeding. In the fitting process, the lineshapes of all six transitions were fitted separately in different windows. In this analysis, we assumed the independent side feeding model for side feeding.

The lifetimes of the nuclear levels of interest were extracted from these shapes using the program LINESHAPE [80]. The lifetimes were obtained by minimizing χ^2 obtained from a comparison of theoretical line shapes, generated by the program LINESHAPE, and experimental line shapes. It is interesting to note that corresponding $B(M1)$ values across the transitions depopulating $I = 14^{(-)}$ state onward in band 1 show almost constant value. This is indicative that the band is not characterized by magnetic rotation, even though ^{92}Nb lies close to the semi-magic core. The transitions are rather characterized by transitions with enhanced magnetic character. Since the parity across the 1550.3-keV transition is tentative, it was imperative to check both $B(E1)$ and $B(M1)$ values. The $B(M1)$ value is excessively low compared to the other members of band 1 whereas $B(E1)$ value to comparable to other neighboring nuclei. Hence, this may be another indicator for assigning tentative negative parity to $I = 14\hbar$ state.

Table 6.1 Measured lifetimes of states in the $M1$ band, τ (ps), and corresponding $B(M1)$ μ_N^2 reduced transition strengths. Systematic errors due to uncertainties in the stopping powers used are not included.

E_γ (keV)	$J_i^\pi \rightarrow J_f^\pi$	Internal conversion coefficient (ICC)	τ ps	$B(M1)^a$ μ_N^2
1550.3	$14^{(-)} \rightarrow 13^+$	100	$0.74^{+0.15}_{-0.15}$	$B(E1)^b = 2.3^{+0.4}_{-0.5} \times 10^{-4} e^2 fm^2$
1550.3	$14^{(+)} \rightarrow 13^+$	100	$0.74^{+0.15}_{-0.15}$	$0.020^{+.003}_{-.005}$
610.1	$15^{(-)} \rightarrow 14^{(-)}$	80	$0.57^{+.73}_{-.40}$	$0.35^{+0.20}_{-0.75}$
580.2	$16^{(-)} \rightarrow 15^{(-)}$	69	$0.47^{+0.43}_{-0.24}$	$0.43^{+0.21}_{-0.44}$
674.8	$17^{(-)} \rightarrow 16^{(-)}$	68	$0.80^{+0.50}_{-0.50}$	$0.16^{+0.07}_{-0.26}$
513.4	$18^{(-)} \rightarrow 17^{(-)}$	100	$0.64^{+0.76}_{-0.22}$	$0.65^{+0.35}_{-0.35}$
718.7	$19^{(-)} \rightarrow 18^{(-)}$	63	$0.58^{+0.24c}_{-0.23}$	$0.17^{+0.06}_{-0.10}$

[a] $B(M1)(expt.)$=0.05697(B.R/100)/$(E\gamma)^3\tau(1+\alpha)$

[b] $B(E1)(expt.)$=6.29(B.R/100)/$(E_\gamma)^3\tau(1+\alpha)$

where E_γ is the experimentally measured transitional energy in units of MeV, τ is the mean lifetime of the decaying level in ps.

[c] Effective lifetime is obtain assuming 100% side-feeding intensity. Hence it is the upper limit of level lifetime (τ).

[d] Lower limit of the $B(M1)$ value.

6.4 Discussions

6.4.1 Shell model calculations

The study of low-lying states in ^{92}Nb has provided valuable insights about the features of a spherical nucleus that can effectively be modelled using the shell model. However, the generation of high-spin states requires the occupation of high-j shape-driving orbits, which may cause the nucleus to become deformed. The resulting deformation presents a challenge to the application of the shell model calculation within a suitably defined valence

space. The same can be anticipated from the shell model calculations by Ren *et al.* [148] where $h_{11/2}$ neutron orbitals have been included in addition to the valence space suggested by Zheng *et al.* [10]. However, involvement of $h_{11/2}$ orbitals at low deformation in the $A \sim 90$ should be less favorable. The last valence neutrons above N=50 were allowed to occupy the $d_{5/2}$ or $g_{7/2}$ or $h_{11/2}$ orbital; whereas the $d_{3/2}$ and $s_{1/2}$ neutron orbitals were not included [148]. In the SNET interaction, the single-particle energy of $\nu(h_{11/2})$ orbital is taken to be less than any other neutron orbital. But, the $\nu(h_{11/2})$ orbital keeps higher single-particle energy compared to the other neutron orbitals ($d_{5/2}$, $d_{3/2}, s_{1/2}$, and $g_{7/2}$) in other regular shell model interactions. In the case of ^{92}Nb, we have single-neutron above N=50, so it will be more logical to choose the model space which includes neutron orbitals $d_{5/2}$, $g_{7/2}$, $s_{1/2}$, and $d_{3/2}$ instead of the higher lying $\nu(h_{11/2})$ orbital. When the energy of the states for second levels across a given spin is calculated by Zheng *et al.* and Ren *et al.*, is compared the agreement with the experimental excitation energy is found to be far better in the former. Nevertheless, as mentioned earlier, most of the available literature in this mass region describes the medium and high-spin regime within the shell-model approach which may not be sufficient in light of the present anomalies. On the contrary, studies of the high-spin region within an appropriate collective model may provide the opportunity to explore the influence of deformation on nuclear structure and shape. Owing to the proximity to the semi-magic core, the high-spin states in ^{92}Nb should be prone to competing effects between single-particle and collective behavior which demands an extensive study of such states through the collective model. This will help us to compare the outcomes with the results of shell-model calculations done earlier (see the discussion in next section on CNS model calculations). The present work is based on the cranked Nilsson Strutinsky model (CNS) that may be considered to be more descriptive compared to the shell model at the high-spin domain due to the limitations of the dimension of model space in shell model calculations at high spins. CNS also has the added benefit of obtaining results as a function of the observable parameter spin, unlike other collective models where the independent variable is the rotational frequency [36, 117, 162, 200].

Owing to the above-mentioned anomalies in shell model results in some of the recent works, systematic shell-model calculations are performed using GWBXG effective interaction with ^{68}Ni core. The last valence neutron was allowed to occupy in any of the neutron-shell $\nu(g_{7/2})$, $\nu(d_{5/2})$, $\nu(d_{3/2})$ and $\nu(s_{1/2})$ orbitals above the $N = 50$. No truncation is employed for proton orbitals $f_{5/2}pg_{9/2}$. The results are summarized in Table A.6. In band 1 the states with I = $14^{(-)}$, $1^{(-)}$, $16^{(-)}$, $17^{(-)}$, and $18^{(-)}$ are produced at comparable excitation energy (deviation is of the order of 400-500 keV only) as observed experimentally while a large gap is observed in the calculated result at I = $19^{(-)}$ and beyond. The corresponding configurations with the highest probability is $\pi((f_{5/2}p)^9 g^4_{9/2}) \otimes \nu(p^2_{1/2} g^{10}_{9/2}(gd)^1)$. On the other hand, subsequent excitation of the protons is observed from the $f_{5/2}p$ shell to the $p_{1/2}$ for levels at I = $19^{(-)}$ to $20^{(-)}$. Similarly, the negative parity band 2 can be assigned proton-excited configurations. The results agree well with the calculated results of Zheng *et al.*. It will be interesting to compare these results in the framework of a collective model.

6.4.2 cranked Nilsson Strutinsky calculations

According to Saha *et al.*, the high-spin negative parity band in ^{89}Zr was observed as a result of the rotation of the nucleus around the possible longest principal axis. Such rotations are classically forbidden and hence, it was interesting to observe such rotation at high-spin states [7]. In the principal axis cranking calculations, the nucleus can rotate around any of the three principal axes corresponding to three different minima for the total energy in the (ε_2, γ) plane. Variation of $\gamma = 0^\circ \rightarrow +60^\circ$ represents rotation of nucleus around the shortest principal axis, $\gamma = 0^\circ \rightarrow -60^\circ$ represents rotation of nucleus around the intermediate axis and = $-60^\circ \rightarrow -120^\circ$ represents rotation around the longest principal axis.

The collective property of ^{92}Nb at the spin state of 14^- and the negative parity $M1$ band built on the said state in the framework of the variable moment of the inertia model (VMI) [148] has been discussed by Ren *et al.*. It is claimed that the model reproduces the

observed regular structure at the mentioned spin in the given nucleus. Based on the model calculation, an oblate shape is predicted for the band. The prediction is largely based on a similar conclusion in ^{93}Nb [152]. The corresponding band in ^{93}Nb was predicted to have an oblate shape based on comparison with ^{131}La where similar conclusions were made based on the cranked shell model (CSM) [160]. Details about the predicted shape in ^{93}Nb have already been discussed in Chapter 5 [111].

In light of the above shortcomings, it becomes further imperative to review and establish the high-spin levels in ^{92}Nb within the framework of the CNS model. The success of the CNS model in describing shape evolution in ^{89}Zr as a function of angular momentum drives us to carry out CNS model-based calculations at a high-spin regime in ^{92}Nb which has three(one) valence protons above Z = 38(40) subshell closure and one valance neutron above N = 50 sub-shell closure. It is to be noted that ^{92}Nb is a particle-dominating nucleus while ^{89}Zr is a hole-dominating nucleus. As a result, ^{92}Nb should prefer to possess rotation around either the shortest principal axis or the intermediate principal axis.

The high-spin states in ^{92}Nb have been probed through the framework of pairing independent cranked Nilsson-Strutinsky (CNS) model [36, 117, 162, 200]. In this model, the configurations are labelled by the number of particles(holes) in the orbitals corresponding to a given N oscillator shell. Further subdivisions are made into high- and low- j shells, where further classifications can be made based upon signature α = 1/2 and α = -1/2.

The calculations are performed with κ and μ parameters fitted for the A = 90 regions [163]. These define the coefficients of the $\mathbf{l}\cdot\mathbf{s}$ and $\mathbf{l}^2$ terms in the modified oscillator potential [94]. The shell energy is extracted using the Strutinsky shell correction formalism [97, 127]. Whereas the total energy is calculated as the sum of the rotating liquid drop energy and the shell energy. Lublin-Strasbourg drop (LSD) [164] has been used as the static liquid drop reference. The rigid body moment of inertia is calculated with a radius parameter of r_0 = 1.16 fm and diffuseness of a = 0.6 fm [117]. The calculations minimize

the total energy across different angular momentum states for the different configurations with respect to the axial and triaxial deformation parameters, ε_2, ε_4, and γ respectively.

The configurations are labelled as per the nomenclature: $[p_1p_2, n_1n_2]$, where, p_1 is the number of proton holes in the *fp* shell and p_2 represents the number of protons in the $g_{9/2}$ shell. As well, n_1 is the number of neutron holes in the $g_{9/2}$ shell, and n_2 shows the number of neutrons in *gds* orbitals. For a complete description of a configuration, the signature in the subshells or group of subshells must be specified. Thus, for an odd number of particles in a group, the signature might be given by a subscript, + for the signature α = 1/2 and - for α = -1/2. In the following, we will discuss the results of the model calculation. The results are then compared with the experimental observations.

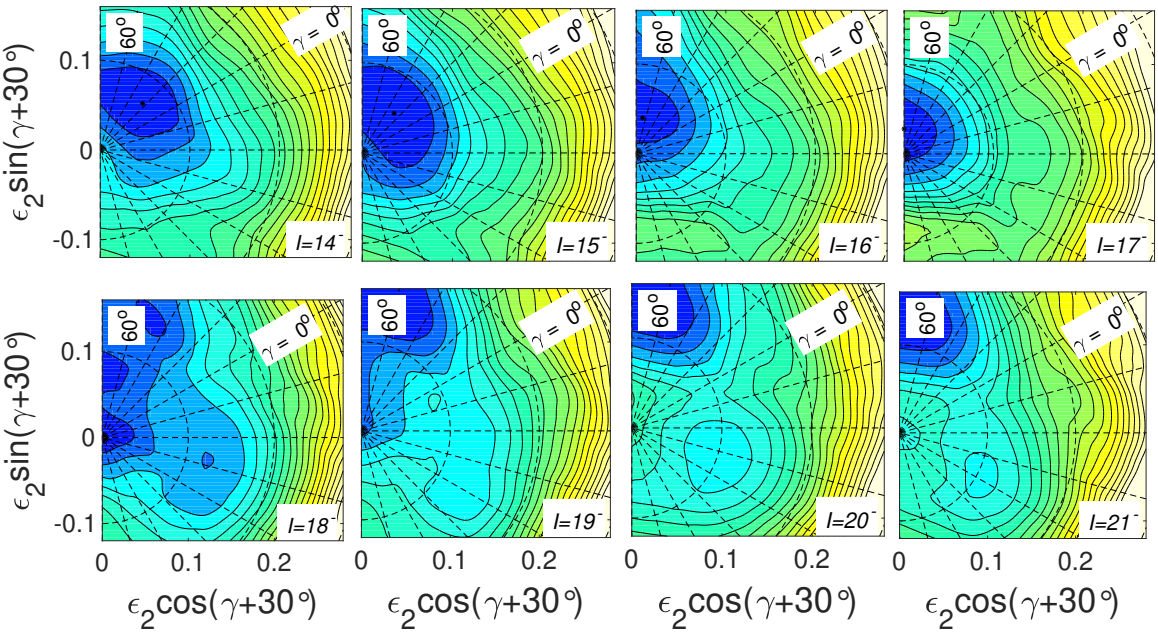

Figure 6.10 Total energy surfaces for general scan run for a spin $14\hbar$ to $21\hbar$ in ^{92}Nb. The contour line separation is 0.25 MeV.

Stable minima in potential energy contours minimized with respect to deformation parameters viz. ε_2, ε_4 and γ are followed as a function of spin ($14\hbar$ to $21\hbar$). (see Fig 6.10). Up to spin $I = 18\hbar$ (except $I = 14\hbar, 15\hbar$) the energy minimum is centred around a non-collective oblate shape with a small $\varepsilon_2 \approx 0.05$ axial deformation parameter. This is characteristic of non-collective behavior, which ideally explains shell model excitations in

the semi-magic nucleus ^{92}Nb. At spin $I = 14\hbar$ and $15\hbar$ the shape is stabilized with $\gamma \approx 15^{\circ}$ and $\varepsilon_2 \approx 0.05$. At $I = 18\hbar$, different minima originate in the contour mesh, indicating the contribution from other configurations. At and beyond $I = 19\hbar$, the ε_2 attains a higher value of ≈ 1.5.

Being a near semi-magic nucleus with 41 protons and 51 neutrons, the shell model type of excitations should be present in ^{92}Nb up to a comparatively large spin range. The above energy minima as a function of deformation parameters are at par with the expected observation. Let us probe into some of the energetically favorable configurations calculated within the above stable energy minima. The excitation energy relative to a rotating liquid drop as a function of spin is shown in Fig. 6.11

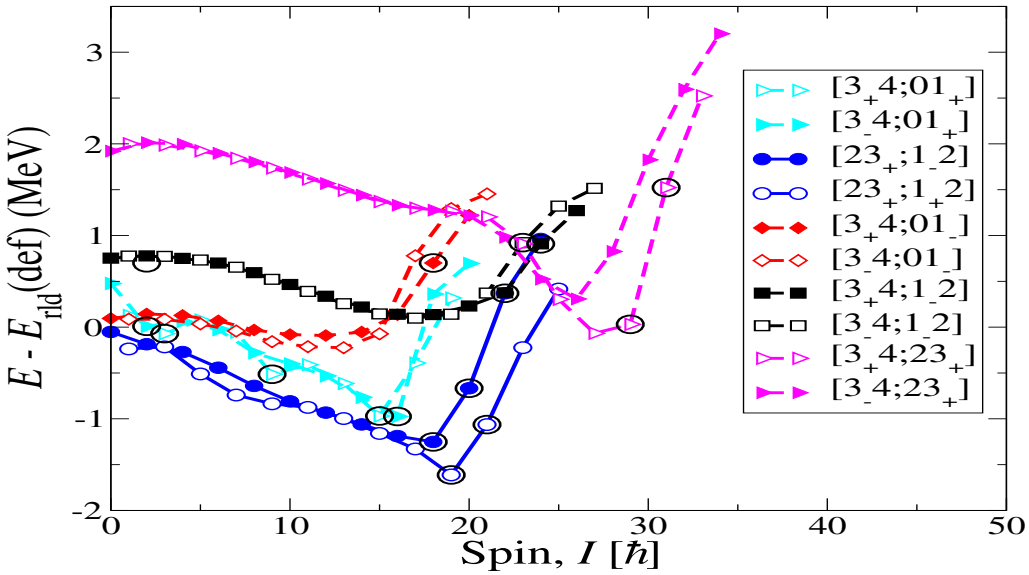

Figure 6.11 Calculated excitation energy relative to rotating liquid drop energy as a function of spin for negative and positive-parity states in ^{92}Nb.

Specific configurations across the PES minima are probed to look for agreement with the experimental observations. The positive-parity configuration [23;12] is lowest in energy up to 19^{+} state. The configuration [23;12] represents two proton holes in fp shell along with three protons in $g_{9/2}$ shell, whereas one neutron hole in $g_{9/2}$ orbital is accompanied by two neutrons in gds shell.

Configurations [34;01] with three proton holes in fp shell, and four protons in $g_{9/2}$ orbitals coupled with one neutron in gds shell are the energetically most favorable negative-parity state at low spin up to $15\hbar$. Bands in ^{92}Nb are observed from $14\hbar$ onward. Hence, this configuration cannot be considered. It is observed that the negative parity configuration $\pi((fp)^{-3}g_{9/2}^{4}) \otimes \nu(g_{9/2}^{-1}(gds)^{2})$ [34;12] remains energetically favorable up to spin $20\hbar$. The variation of excitation energy as a function of spin is not quite smooth, and this may be attributed to non-collective excitation within the near semi-magic nucleus.

A few more negative parity configurations are shown in the given figure, though they lie at higher excitation energy compared to [34;12]. For the sake of completeness, a configuration [34;23] $\pi(fp)^{-3}(g_{9/2}^{4}) \otimes \nu(g_{9/2}^{-2}(gds)^{3})$ was also displayed, which can be built up to $34\hbar$ maximum spin. This configuration may be useful in describing higher excitation states in the nucleus. Some of the favorable configurations were selected and compared with the observed bands in Fig. 6.12. Experimental excitation energy relative to rotating liquid drop for different level structures, as mentioned in the level scheme (see Fig. 6.1), is plotted as a function of spin in the uppermost panel of Fig. 6.12. The same for the various configurations obtained from the CNS calculations are shown in the middle panel of Fig. 6.12. They are compared and the difference between the calculated and experimental results is displayed in the lowermost panel of Fig. 6.12.

A couple of bands, with negative parity (band 1 and band 2), are observed experimentally which are characterised by intra-band dipole transitions. If compared with the neighboring ^{89}Zr [145], ^{90}Y [6] and ^{93}Nb [111], these two bands should be the potential candidate to study the rotational features of the nucleus. It is to be mentioned that for clarity of calculation, the even-spin states (closed symbols) of bands 1 and 2 are displayed as 1a and 2a bands, whereas the odd-spin (open symbols) are shown as 1b and 2b bands, respectively.

Now, the even- and odd-spin states of band 1 were compared with configurations suggested by Zheng *et al.* $[3_{-}4;01_{+}]$ and $[3_{+}4;01_{+}]$ respectively. It is seen that configuration

[34;01] is not in good agreement with the experiment, as the difference between the two is up-sloping over the given spin range.

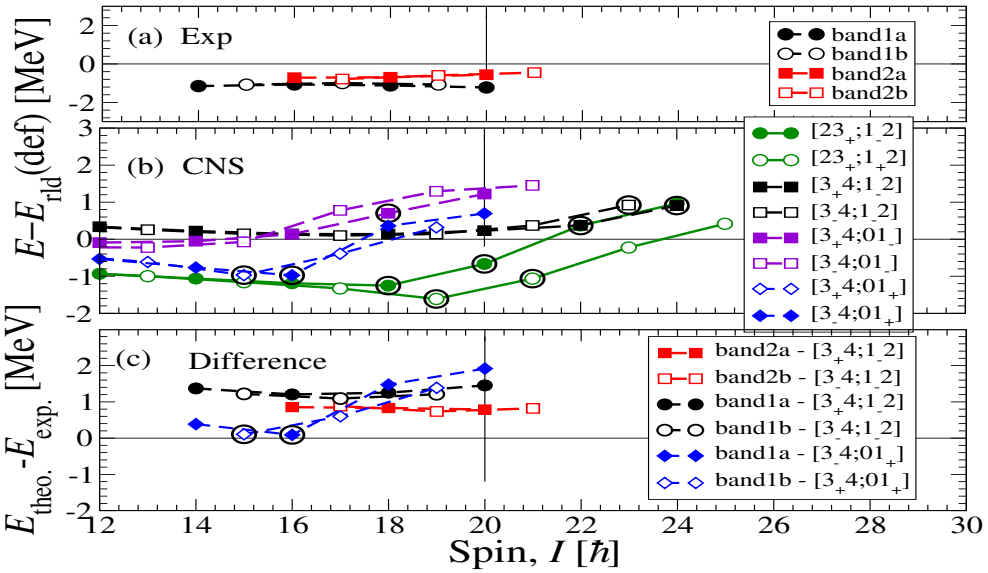

Figure 6.12 Excitation energies relative to rotating-liquid drop energy as a function of angular momentum, for observed (panel a) and calculated (panel b) valence-space states for ^{92}Nb. The difference between the observed and calculated results is shown in panel c.

Further, band 1 and band 2 are compared with [34;12] configuration. The even- and odd-spin states are compared with configurations, $[3_-4;1_+2]$ and $[3_+4;1_+2]$ respectively. Both the bands 1 and 2 agrees well with $[3_-4;1_+2]$ and $[3_+4;1_+2]$ over the given spin range as the difference between the two stays almost constant at 1 and 1.5 MeV respectively.

Now, let us probe into the shapes of this configuration as a function of spin. The surface plots (see Fig. 6.13) show that the shape is stabilized with $\gamma \approx$ -20° up to spin 21$\hbar$. This concludes that bands 1 and 2 represent the rotation around the intermediate principal axis. The value of ε_2 varies from $\approx$ 0.15 to $\approx$ 0.10 as spin increases from 14$\hbar$ to 21$\hbar$.

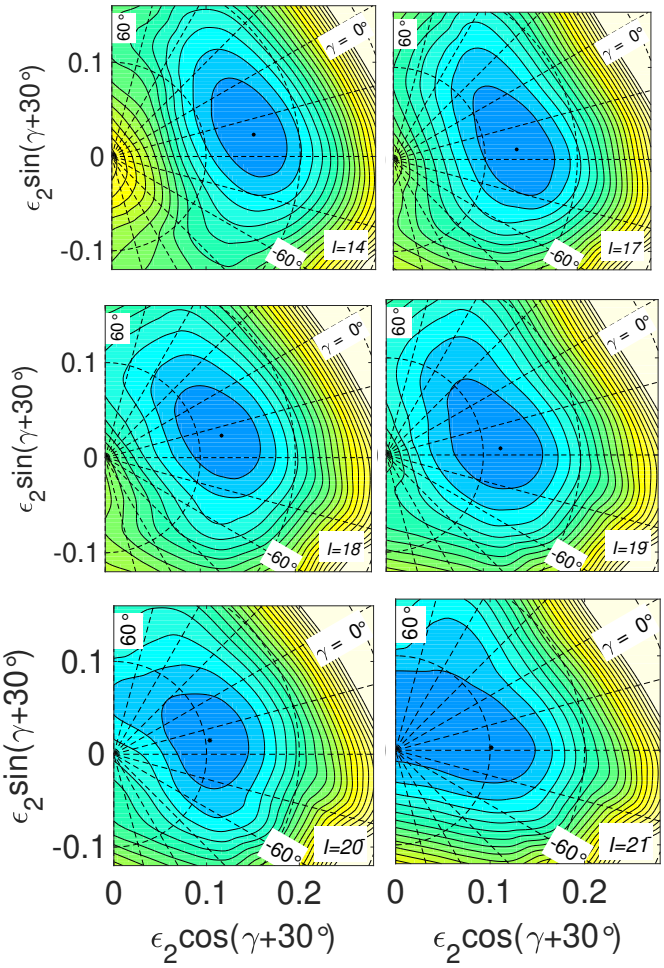

Figure 6.13 Calculated total energy surfaces for $14\hbar$, $17\hbar$, $18\hbar$, $19\hbar$, $20\hbar$, $21\hbar$ for [34;12] in ^{92}Nb.

6.5 Summary

The level scheme of ^{92}Nb has been expanded with the placement of twenty-nine new transitions and the repositioning of a few already reported transitions. A couple of already observed dipole bands have been placed with connecting transitions, and a new dipole band has been placed. In particular, band 1 has been shown to feed on low-spin levels. Such bands have already been reported in several other nuclei in the given mass region. Spins and parities assignment has been done through measurement of ADO ratios and polarization asymmetries of γ rays. Feasible configurations of band 1 which were previously analyzed by Zheng *et al*. [10] and the newly observed band 2 are discussed within the framework of both the shell model calculations and CNS model. According to the CNS calculations, the lowest-energy configuration which can explain band 1 and band 2 are built with four protons in $g_{9/2}$ orbital and two neutrons excited across the $N = 50$ shell gap to *gd* shells, i.e., [34;12]. Detailed calculations show that the configuration [34;12] represents the triaxial shape for most of the observed spin range with$\gamma \approx$ -20°, $\varepsilon_2 \approx 0.15$. On the other hand, the shell model results predict a configuration based on completely filled $g_{9/2}$ neutron orbitals for both band1 and band2, respectively. This may be attributed to the lack of pairing interaction in the CNS model. Thus, observation of dipole bands in nuclei neighboring to semi-magic core provides a platform to understand the contribution of alignment of particles as well as holes towards driving the nuclei to rotate about different principal axes.